Available online at www.sciencedirect.com
SCIENCE DIRECT®
International Journal of Mass Spectrometry 241 (2005) 75–81
International Journal of Mass Spectrometry
www.elsevier.com/locate/ijms

Bond strengths in $POCl_3^-$, $POCl_2^-$, and $PSCl_2^-$

Kim C. Lobring[a], Catherine E. Check[b], Mary L. Boggs[a], Pamela R. Keating[a], Lee S. Sunderlin[a,*]

[a] *Department of Chemistry and Biochemistry, Northern Illinois University, DeKalb, IL 60115, USA*
[b] *Department of Sciences, Rock Valley College, 3301 North Mulford Road, Rockford, IL 61114, USA*

Received 8 December 2003; accepted 25 October 2004
Available online 8 December 2004

Abstract

The bond strengths $D(OCl_2P^-–Cl) = 172 \pm 7$, $D(OClP–Cl^-) = 177 \pm 8$, and $D(SClP–Cl^-) = 186 \pm 6$ kJ mol^{-1} have been determined at 0 K by measuring thresholds for collision-induced dissociation in a flowing afterglow-tandem mass spectrometer. This thermochemistry is consistent with a close balance between dissociative and nondissociative electron capture for $POCl_3$ and $PSCl_3$. B3LYP and G3 computational results give bond strengths lower by an average of about 20 kJ mol^{-1}.

Keywords: Radical ions; Electron capture; Thermochemistry; Computational chemistry

1. Introduction

Phosphoryl chloride, $POCl_3$, is used extensively (hundreds of kilotons per year) [1] as a precursor for a variety of organophosphorus compounds. $POCl_3$ has also been found to be an effective electron scavenger in flames [2]. Electron capture by $POCl_3$ produces $POCl_3^-$ as well as two dissociative products, Cl^- and $POCl_2^-$ (reactions 1–3) [3,4]. The degree of dissociation is sensitive to the temperature and pressure of the electron capture conditions. In contrast, $PSCl_3$ produces only dissociative products, Cl^- and $PSCl_2^-$ (reactions 4 and 5), except at relatively high pressures [5].

$$POCl_3 + e^- \rightarrow POCl_3^- \quad (1)$$

$$POCl_3 + e^- \rightarrow POCl_2 + Cl^- \quad (2)$$

$$POCl_3 + e^- \rightarrow POCl_2^- + Cl \quad (3)$$

$$PSCl_3 + e^- \rightarrow PSCl_2 + Cl^- \quad (4)$$

$$PSCl_3 + e^- \rightarrow PSCl_2^- + Cl \quad (5)$$

Understanding the product distributions depends on understanding the thermochemistry of the possible products, but some of the necessary data is not well known. The electron affinities of $POCl_2$ and $POCl_3$ were measured to be 3.83 and 1.41 eV by determining the thresholds for anion formation upon charge transfer from Cs to $POCl_3$ [6]. The corresponding values calculated at the G2 level (3.71 and 1.50 eV) [7] and G3 level (3.73 and 1.59 eV) [8] are in reasonable agreement with the experimental results. G3 calculations have also been performed on $PSCl_2$, $PSCl_3$, and their anions [5], but experimental results are lacking.

The substitution of sulfur for oxygen in $POCl_3$ must affect the thermodynamics in order to cause the differences in the product distributions. A substantial amount of theoretical work on the nature of P–O and P–S bonding has been performed [9–13]. Most of the results are consistent with a picture of a $P^+–O^-$ single bond with some backbonding, while the sulfur analog is less polarized.

We have performed collision-induced dissociation experiments on $POCl_3^-$, $POCl_2^-$, and $PSCl_3^-$ to determine thermochemistry that can provide additional insight into these systems. A related study of $POCl_4^-$ and $PSCl_4^-$ has also been completed recently [14]. An advantage of these gas-phase

* Corresponding author. Tel.: +1 815 753 6870; fax: +1 815 753 4802.
E-mail address: sunder@niu.edu (L.S. Sunderlin).

1387-3806/$ – see front matter © 2004 Elsevier B.V. All rights reserved.
doi:10.1016/j.ijms.2004.10.023

experiments is that the effects of solvation on the bonding [15] are eliminated, making the experimental results directly comparable to computational results.

2. Experimental

Bond strengths were measured using the energy-resolved collision-induced dissociation (CID) technique [16,17] in a flowing afterglow-tandem mass spectrometer (MS) [18]. The instrument consists of an ion source region, a flow tube, and the tandem MS. The DC discharge ion source used in these experiments is typically set at 2000 V with 2 mA of emission current. The flow tube is a 92 cm × 7.3 cm i.d. stainless steel pipe that operates at a buffer gas pressure of 0.35 Torr, a flow rate of 200 standard $cm^3\ s^{-1}$, and an ion residence time of 100 ms. The buffer gas is helium with up to 10% argon added to stabilize the DC discharge.

To make $POCl_3^-$ and $POCl_2^-$ for this study, $POCl_3$ was added to the ion source. The main ion produced under our experimental conditions is $POCl_3^-$. The main products of direct electron impact on $POCl_3$ are $POCl_2^-$, $POCl_3^-$, and a small amount of Cl^- [4]. The experiments of Knighton et al., where branching ratios are measured, were done at low reagent flow conditions to minimize secondary reactions. Higher flow rates were used in the present experiments to maximize production of the desired reagent ions. Thus, secondary reactions have a significant impact on the ion distribution. Substantial amounts of $POCl_4^-$ are also created, as discussed previously [14]. Approximately 10^5 collisions with the buffer gas cool the metastable ions to room temperature.

$PSCl_3$ was the precursor for $PSCl_2^-$. Electron attachment to $PSCl_3$ at the pressures used in these experiments gives only dissociative products [5], although it may be possible to produce $PSCl_3^-$ from secondary reactions. Attempted experiments on $PSCl_3^-$ were inconsistent, probably because it is very difficult to cleanly separate the desired ions (which have a wide isotope distribution) from other ions with overlapping mass spectra. Therefore, only computational results for $PSCl_3^-$ will be discussed in this paper.

The tandem MS includes a quadrupole mass filter, an octopole ion guide, a second quadrupole mass filter, and a detector, contained in a stainless steel box that is partitioned into five interior chambers. Differential pumping on the five chambers ensures that further collisions of the ions with the buffer gas are unlikely after ion extraction. During CID experiments, the ions are extracted from the flow tube and focused into the first quadrupole for mass selection. The reactant ions are then focused into the octopole, which passes through a reaction cell that contains a collision gas (argon in the present experiments). After the dissociated and unreacted ions pass through the reaction cell, the second quadrupole is used for mass analysis. The detector is an electron multiplier operating in pulse-counting mode.

The energy threshold for CID is determined by modeling the cross section for product formation as a function of the reactant ion kinetic energy in the center-of-mass (CM) frame, E_{cm}. The octopole is used as a retarding field analyzer to measure the reactant ion beam energy zero. The ion kinetic energy distribution for the present data is typically Gaussian with an average full-width at half-maximum of 0.8–1.1 eV (1 eV = 96.5 kJ mol^{-1}). The octopole offset voltage measured with respect to the center of the Gaussian fit gives the laboratory kinetic energy, E_{lab}, in eV. Low offset energies are corrected for truncation of the ion beam [19]. To convert to the CM frame, the equation $E_{cm} = E_{lab}m(m+M)^{-1}$ is used, where m and M are the masses of the neutral and ionic reactants, respectively. All experiments were performed with both mass filters at low resolution to improve ion collection efficiency and reduce mass discrimination. Average atomic masses were used for all elements.

The total cross section for a reaction, σ_{total}, is calculated using Eq. (6), where I is the intensity of the reactant ion beam, I_o is the intensity of the incoming beam ($I_o = I + \Sigma I_i$), I_i is the intensity of each product ion, n is the number density of the collision gas, and l is the effective collision length, 13 ± 2 cm. Individual product cross sections σ_i are equal to σ_{total} $(I_i/\Sigma I_i)$. Data taken at several pressures is extrapolated to a zero pressure cross section before fitting the data to avoid the effects of secondary collisions [20].

$$I = I_o \exp(-\sigma_{total} n l) \tag{6}$$

Threshold energies are derived by fitting the data to a model function given in Eq. (7), where $\sigma(E)$ is the cross section for formation of the product ion at CM energy E, E_T is the desired threshold energy, σ_o is the scaling factor, n is an adjustable parameter, and i denotes rovibrational states having energy E_i and population g_i ($\Sigma g_i = 1$). Doppler broadening and the kinetic energy distribution of the reactant ion are also accounted for in the data analysis, which is done using the CRUNCH program written by Armentrout and coworkers [19].

$$\sigma(E) = \frac{\sigma_o \sum_i g_i (E + E_i - E_T)^n}{E} \tag{7}$$

Experimental vibrational frequencies are not available for the anions studied in this work. Therefore, vibrational and rotational frequencies were calculated using the B3LYP/aug-cc-pVTZ model to give a consistent set of frequencies, given in Table 1. The calculated frequencies reported here for POCl and PSCl average 2% lower than experiment, which is typical for this type of system [14,21]. Recent work on closely related molecules with this model suggests it gives generally good agreement with experiment [22]. Therefore, the calculated frequencies were used without scaling. Uncertainties in the derived thresholds due to possible inaccuracies in the frequencies were estimated by multiplying the entire sets of frequencies by 0.9 and 1.1. The resulting changes in internal energies are less than 2 kJ mol^{-1}. Polarizabilities for neutral molecules were also taken from the computational results; varying these parameters has a negligible effect on the derived bond strengths.

Table 1
Vibrational frequencies and rotational constants[a]

Compound	Experimental vibrational frequency (cm^{-1})	Calculated vibrational frequency (cm^{-1})[b]	Rotational frequency (cm^{-1})[b]	Polarizability (10^{-24} cm^3)[b]
$POCl_3^-$		23.7	0.0337	
		28.4	0.0518	
		142	0.0525	
		184		
		185		
		266		
		393		
		394		
		1237		
$POCl_2^-$		125	0.0543	
		201	0.0764	
		252	0.1469	
		335		
		395		
		1203		
$POCl_2$		180	0.0602	
		263	0.0877	
		308	0.1682	
		453		
		508		
		1209		
$PSCl_2^-$		135	0.0427	
		154	0.0771	
		210	0.0786	
		304		
		351		
		631		
POCl	308[c]	297	0.1287	6.28
	489[c]	479	0.1460	
	1263[c]	1277	1.086	
PSCl	229[d]	220	0.0800	9.25
	462[d]	442	0.0921	
	716[d]	717	0.6062	
Cl		–	–	2.19

[a] Numbers in parentheses are degeneracies.
[b] Present work, calculated at the B3LYP/aug-cc-pVTZ level.
[c] Ref. [22].
[d] Ref. [37].

Collisionally activated metastable complexes can have long enough lifetimes that they do not dissociate on the experimental timescale (ca. 50 μs). Such kinetic shifts are accounted for in the CRUNCH program by RRKM lifetime calculations, where the reaction transition states are presumed to be essentially product-like [23]. The uncertainty in the derived thresholds is again estimated by multiplying reactant or product frequency sets by 0.9 and 1.1, and by multiplying the time window for dissociation by 10 and 0.1. The effect of these variations is less than 2 kJ mol^{-1}.

The reagents $POCl_3$ and $PSCl_3$ were obtained from Aldrich. He and Ar were obtained from BOC. All reagents were used as received.

Computational work on these systems was performed using the Gaussian 98 Suite [24]. The Natural Bond Orbitals Analysis (NBO) [25] program was used to study the charge distributions in these systems.

3. Results

CID of $POCl_3^-$ gives loss of Cl atom, reaction 8, as the predominant product. Reactions 9 and 10 were also observed. In reaction 9, $POCl_2$ may instead be the dissociated products (POCl + Cl). Appearance curves for CID of $POCl_3^-$ are shown in Fig. 1. The observed predominance of chlorine atom loss is consistent with $POCl_2$ having a slightly higher electron affinity than Cl [6].

$$POCl_3^- \rightarrow POCl_2^- + Cl \quad (8)$$

$$POCl_3^- \rightarrow POCl_2 + Cl^- \quad (9)$$

$$POCl_3^- \rightarrow POCl + Cl_2^- \quad (10)$$

$POCl_2^-$ and $PSCl_2^-$ both give loss of Cl^- as the only major CID product, reactions 11 and 12. With $PSCl_2^-$, about 0.2% of what is apparently a Cl_2^- product ion was also observed. This trace product will not be considered further. The appearance curves are shown in Figs. 2 and 3.

$$POCl_2^- \rightarrow POCl + Cl^- \quad (11)$$

$$PSCl_2^- \rightarrow PSCl + Cl^- \quad (12)$$

Ideally, it would be possible to use modeling software developed to simultaneously determine the thresholds for two competing reactions to determine the relative energetics of reactions 8 and 9 [26]. Attempts at fitting the data failed to match the observed cross sections. A possible reason for the unsuccessful competitive fit is incorrect calculated densities of states for the transition states, which as noted above are believed to be product-like. This is more likely for systems such as $POCl_3^-$, where the reactant and both polyatomic products

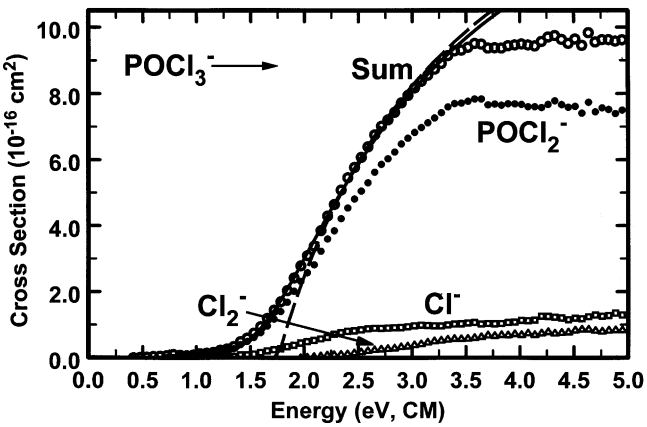

Fig. 1. Cross section for collision-induced dissociation of $POCl_3^-$ as a function of energy in the CM frame. The solid and dashed lines represent convoluted and unconvoluted fits to the data, as discussed in the text.

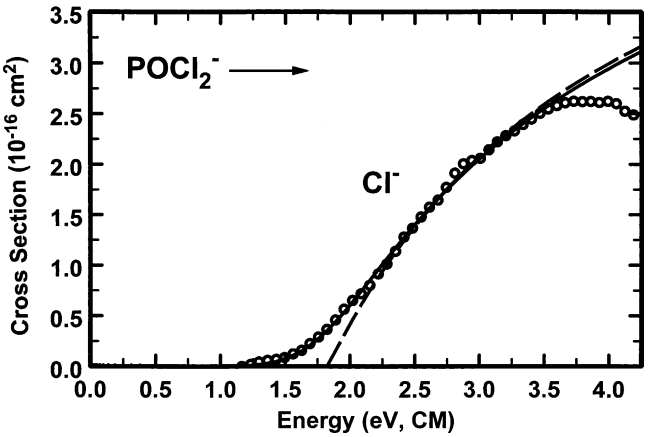

Fig. 2. Cross section for collision-induced dissociation of $POCl_2^-$ as a function of energy in the CM frame. The solid and dashed lines represent convoluted and unconvoluted fits to the data, as discussed in the text.

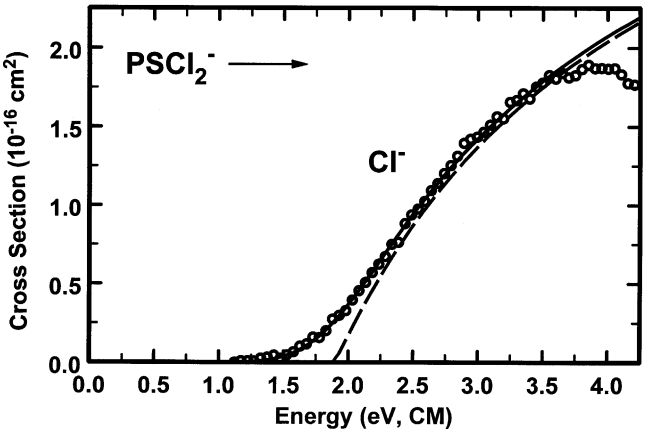

Fig. 3. Cross section for collision-induced dissociation of $PSCl_2^-$ as a function of energy in the CM frame. The solid and dashed lines represent convoluted and unconvoluted fits to the data, as discussed in the text.

have very low vibrational frequencies that may not be harmonic at higher energy levels. Competitive fits do support the qualitative observation that the electron affinity of $POCl_2$ is slightly higher than that of Cl.

The data for $POCl_3^-$ was therefore fit with a model involving a single reaction channel. There are two limiting cases for modeling this dissociation. One case assumes that formation of the minor products does not deplete the collisionally activated ions that would otherwise dissociate to form the main product, $POCl_2^-$. In this situation, the data for formation of the main product (reaction 8) should be fit using the transition state parameters for that reaction. The second case is that all formation of the minor products *does* deplete an intermediate that leads to the main product. This includes the possibility that some of the products of reactions 9 or 10 are secondary products formed after initial dissociation of a chlorine atom. In this case, the *total* cross section should be fit with the parameters for reaction 8. These two procedures give a negligible difference in the derived thermochemistry, <1 kJ mol^{-1}, and the fitting parameters (Table 2) are the same. Thus, the uncertainty in the dissociation pathways has an insignificant effect on the derived thermochemistry.

There are two reasons that these derived thresholds are essentially the same. One is that the main product cross-section has nearly the same shape as the total cross section (the main product is about 85% of the total cross section at threshold and declines slowly to about 75%). The other is that for the relatively small molecule $POCl_3^-$, the kinetic shift is small (less than 0.1 eV). Thus, although the product branching ratios are sensitive to the details of the transition state parameters, the overall threshold is nearly insensitive.

The Eq. (7) fitting parameters for all three systems are given in Table 2, and the fits are shown in Figs. 1–3 as well. The effects of reactant and product internal energy are included in the fitting procedure, so the dissociation thresholds correspond to bond energies at 0 K. The final uncertainties in the bond energies are derived from the standard deviation of the thresholds determined for individual data sets, the uncertainty in the reactant internal energy, the effects of kinetic shifts, and the uncertainty in the energy scale (±0.15 eV lab). These results are given in Table 2.

The experimental 0 K bond energies determined this way can be converted into 298 K bond enthalpies using the integrated heat capacities of the reactants and products, which are determined using the frequencies in Table 1. These give 298 K bond enthalpies that are nearly unchanged (Table 2).

Calculations on the molecules relevant to this study were done using several models and basis sets. The optimized geometries are not very dependent on the basis set chosen. The geometries calculated using B3LYP/aug-cc-pVTZ are given

Table 2
Fitting parameters and bond strengths[a]

Anion	E_T (eV)	n	BDE[b]	BDE[c]	Calculated BDE[d]	Calculated BDE[e]	Calculated BDE
$POCl_3^-$	1.78 ± 0.06	1.0 ± 0.1	172 ± 7	172 ± 7	145	154	155[f]
$POCl_2^-$	1.83 ± 0.07	1.1 ± 0.1	177 ± 8	178 ± 8	155	156	164[g]
$PSCl_2^-$	1.93 ± 0.05	1.0 ± 0.1	186 ± 6	187 ± 6	147	147	161[g]

[a] See text for discussion of fitting parameters. Bond dissociation enthalpies in kJ mol^{-1}.
[b] Value at 0 K.
[c] Value at 298 K.
[d] B3LYP/6-311 + G(d) value at 0 K.
[e] B3LYP/aug-cc-pVTZ value at 0 K.
[f] G3 value at 0 K from ref. [8].
[g] G3 values at 0 K from T.M. Miller, private communication.

Table 3
Predicted (B3LYP/aug-cc-pVTZ level) and experimental (microwave) structural data for $POCl_3$, $PSCl_3$, and related molecules and anions

Species	P—O(S)	P—Cl	O(S)—P—Cl	Cl—P—Cl
$POCl_3$	1.464	2.032	114.8	103.6
exp[a]	1.4464	1.9929	114.91	103.53
$POCl_3^-$ (2)	–	2.302	108.66	110.56
(1)	1.478	2.309	108.62	109.73
$PSCl_3$	1.907	2.052	116.4	101.8
exp[b]	1.8835	2.0093	116.35	102.09
$PSCl_3^-$ (2)	–	2.359	111.2	99.4
(1)	1.949	2.176	110.5	123.3
$POCl_2^-$	1.490	2.307	106.06	96.83
$PSCl_2^-$	1.968	2.271	107.00	96.02
POCl	1.472	2.104	109.88	–
exp[c]	1.462	2.059	110.0	–
exp[d]	1.461	2.060	109.9	–
PSCl	1.912	2.113	110.11	–

Distances are in Å, angles in degrees. Degeneracies are in parentheses.
[a] Ref. [38].
[b] Ref. [39].
[c] Ref. [40].
[d] Ref. [41].

in Table 3, and calculated bond energies are given in Table 2. NBO atomic charges are given in Table 4.

4. Discussion

4.1. Geometries

The calculated geometric parameters for species studied in this paper are given in Table 3, along with the limited experimental data. Other computational results for several of these species have been reported previously [5,8,14], but not at a consistent computational level. The bond lengths calculated with the B3LYP/aug-cc-pVTZ method are slightly longer than the experimental values, which is typical [14,27]. The bond angles are in generally good agreement.

If $POCl_3$ and $PSCl_3$ are assigned formal charges of +1 for the phosphorus and −1 for the oxygen or sulfur atoms, then Lewis structures for these molecules have four electron pairs around each central phosphorus atom. Thus, VSEPR arguments [28] predict nearly tetrahedral structures with threefold symmetry, in agreement with the experimental and computational results. However, the stereochemical effect of the additional electron in $POCl_3^-$ and $PSCl_3^-$ is less easily predicted.

Table 4
Atomic charges and spin densities calculated using MP2/LANL2DZpd and the NBO method (degeneracies in parentheses)

Molecule	q_P	q_{Cl}	$q_{O/S}$	Spin(P)	Spin(Cl)	Spin (O/S)
$POCl_3$	1.658	−0.229	−0.970	–	–	–
$POCl_3^-$	1.430	−0.471	−1.018	0.428	0.188	0.007
$POCl_2^-$	1.137	−0.550	−1.037	–	–	–
POCl	1.236	−0.371	−0.865	–	–	–
$PSCl_3$	0.994	−0.216	−0.345	–	–	–
$PSCl_3^-$	0.803	−0.466 (2) −0.350 (1)	−0.521	0.446	0.216 (2) 0.055 (1)	0.066
$PSCl_2^-$	0.548	−0.470	−0.609	–	–	–
PSCl	0.580	−0.323	−0.257	–	–	–

Begum and Symons [29] measured the ESR spectrum of $POCl_3^-$ in a solid sample of $POCl_3$. They noted that two chlorine atoms had larger hyperfine couplings (66 G) while one was smaller (20 G), which rules out threefold symmetry for $POCl_3^-$. They also noted that the hyperfine coupling for P was 1359 G. The B3LYP/aug-cc-pVTZ value for P (1323 G) is in good agreement, but the values for the chlorine atoms are different (two atoms with 28.7 and one with 28.2 G). The calculated P–Cl bond lengths are identical for two chlorine atoms (2.302 Å) and slightly different for the third (2.309 Å), which is consistent with the small differences in the hyperfine coupling constants. The calculated atomic charges and spin densities for the three chlorine atoms (Table 4) are essentially identical. Fernandez et al., however, calculated a moderate difference in the MP2/6-311+G(d) NBO populations of the chlorine atoms (−0.492 for two atoms and −0.404 for one) [8].

Although experiment and computation both indicate that addition of an electron to $POCl_3$ breaks the threefold symmetry of the chlorine atoms, the computational results suggest that the extra electron is almost stereochemically inactive; all of the bond angles in $POCl_3^-$ are within one degree of the tetrahedral angle of 109.5°. The much greater symmetry breaking in the experimental hyperfine coupling constants could be caused by the solid state environment. For example, the Cl–P–Cl scissors vibrational mode calculated to lie at 28 cm^{-1} breaks the symmetry of the three chlorine atoms; the low frequency indicates that even a weak interaction with neighboring molecules could substantially affect the solid state geometry. Similarly, I_3^-, which has a low asymmetric stretching frequency, is often distorted in crystal structures [30].

$PSCl_3^-$ is calculated to be significantly less symmetric, even in the gas phase. The bond lengths are 2.359 Å (doubly degenerate) and 2.176 Å, and the calculated hyperfine couplings are 1238 G for the P atom, 27.3 G for two Cl atoms, and 12.6 G for one Cl atom. The atomic charges and spin densities in Table 4 reflect this symmetry breaking as well. Very similar atomic charges were previously reported [5].

$POCl_2^-$ and $PSCl_2^-$ have eight electrons around the central P atom, given the assignment of the negative charge to oxygen or sulfur. Therefore, the VSEPR prediction is that the O(S)–P–Cl and Cl–P–Cl angles are somewhat less than the tetrahedral angle of 109.5°. $POCl_2^-$ and $PSCl_2^-$ are calculated to have very similar geometries that agree with these predictions. Since there are three electron clouds around the phosphorus atom in POCl and PSCl, bond angles near 120° are expected, in agreement with the calculations.

4.2. Experimental and theoretical bond energies

Computed bond energies are given in Table 2 with the experimental results. The calculated values are 13–39 kJ mol^{-1}

below experiment; the G3 calculations are in better agreement than the B3LYP calculations. B3LYP/aug-cc-pVTZ calculations of P–Cl^- bond strengths in 10-electron complexes are in good agreement with experiment [14], but corresponding bond strengths in group 14 complexes such as ACl_5^- (A = Si, Ge, Sn) are 10–44 kJ mol^{-1} lower than experimental results [31]. The reason for these inconsistent results is not clear.

The bond strengths measured here allow several comparisons to be made. The bond strengths in $POCl_2^-$ and $PSCl_2^-$ are almost the same, consistent with very similar P–Cl bonding in these systems. The bond strength in $POCl_3^-$ is essentially as strong as the bonds in the closed-shell species $POCl_2^-$ and $PSCl_2^-$. While the reactant is a thermodynamically disfavored radical anion, the chlorine atom product is also a radical. All three bond strengths measured here, however, are substantially stronger than the bond strengths measured [14] in the 10-electron systems $POCl_4^-$ and $PSCl_4^-$ (43 ± 5 and 41 ± 4 kJ mol^{-1}, respectively).

4.3. Heats of formation and electron capture thermodynamics

The thermodynamics of several $POCl_x$ species can be combined to provide additional conclusions, as shown schematically in Fig. 4. The gas-phase heat of formation of POCl has been measured by Dudchik and Polyachenok [32] and Binnewies et al. [33], giving respectively $\Delta_f H_{298}$(POCl, g) = -274 ± 15 kJ mol^{-1} and -251 ± 30 kJ mol^{-1}. These values can be combined with $\Delta_f H_{298}(Cl^-, g) = -229.4$ kJ mol^{-1} [34] and the bond enthalpy determined in this work, D_{298}(POCl–Cl^-) = 178 ± 8 kJ mol^{-1}, to give $\Delta_f H_{298}(POCl_2^-, g) = -681 \pm 17$ kJ mol^{-1} or -658 ± 31 kJ mol^{-1}. These numbers can then be combined with the thermochemistry for reaction 8 and $\Delta_f H_{298}$(Cl, g) = 121.3 kJ mol^{-1} [34] to give $\Delta_f H_{298}(POCl_3^-, g) = -732 \pm 18$ kJ mol^{-1} or -709 ± 32 kJ mol^{-1}. Since $\Delta_f H_{298}(POCl_3, g) = -559.8 \pm 1.7$ kJ mol^{-1} [34], the electron affinity of $POCl_3$ at 298 K can be calculated to be 172 ± 18 kJ mol^{-1} or 149 ± 32 kJ mol^{-1} (1.78 ± 0.19 eV or 1.54 ± 0.33 eV). These values are somewhat higher than the experimental value of 1.41 ± 0.20 eV determined previously [6], but bracket the G3 computational value of 1.59 eV [5].

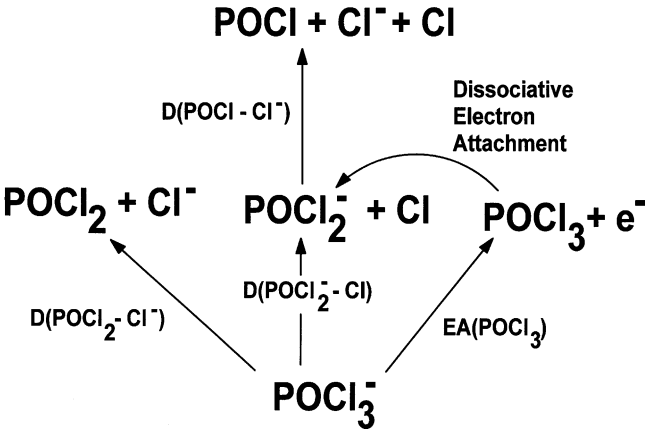

Fig. 4. Reaction energetics scheme for relevant phosphorus oxychlorides.

The experimental results can be used to determine the thermochemistry of dissociative electron attachment more directly by comparing the thermochemistry of the reactants and products of reaction 3, using $\Delta_f H_{298}(e^-, g) = 0.0$ kJ mol^{-1} [34]. The reaction 3 enthalpy is calculated to be 0 ± 17 kJ mol^{-1} or 23 ± 31 kJ mol^{-1}. This supports the calculated G3 results [5], which show that reactions 2 and 3 are endothermic by 11 and 0 kJ mol^{-1}, respectively. The near thermoneutrality is consistent with electron attachment leading to competition between collisional stabilization and dissociation.

The gas-phase heat of formation of PSCl, $\Delta_f H_{298}$(PSCl, g), is -11.9 kJ mol^{-1} (no uncertainties were given for this measurement) [35]. Combining this value with the threshold for reaction 12 and $\Delta_f H_{298}(Cl^-, g) = -229.4$ kJ mol^{-1} [34] gives $\Delta_f H_{298}(PSCl_2^-, g) = -428$ kJ mol^{-1}. This can be combined with $\Delta_f H_{298}(PSCl_3, g) = -292$ kJ mol^{-1} [36] to give an enthalpy for reaction 5 of -15 kJ mol^{-1}. G3 calculations [5] determine enthalpies for reactions 4 and 5 of -20 and -12 kJ mol^{-1}, respectively; the second number is in good agreement with experiment. While the uncertainties in the experimental numbers are large, the greater exothermicity is consistent with electron capture giving more dissociation for $PSCl_3$ than for $POCl_3$. More precise thermochemistry on the neutral molecules involved in the thermochemical calculations would clarify the energetics of electron capture.

5. Conclusions

Collision-induced dissociation of three ions derived from phosphoryl chloride and thiophosphoryl chloride gives bond energies of $D(OCl_2P^-–Cl) = 172 \pm 7$, D(OClP–Cl^-) = 177 ± 8, and D(SClP–Cl^-) = 186 ± 6 kJ mol^{-1}. B3LYP and G3 calculations give bond energies that are lower than experiment. The derived thermochemistry of electron capture for $POCl_3$ and $PSCl_3$ is consistent with theory and electron capture experiments.

Acknowledgments

This material is based upon work supported by the National Science Foundation under grant number 9985883. We thank Peter Armentrout, Mary Rodgers, and Kent Ervin for use of the CRUNCH software for data analysis and the NIU Computational Chemistry Laboratory for computer usage.

References

[1] N. Wiberg, Holleman-Wiberg Inorganic Chemistry, first English ed., Academic Press, San Diego, 2001.

[2] J.H. Horton, P.N. Crovisier, J.M. Goodings, Int. J. Mass Spectrom. Ion Processes 114 (1992) 99.
[3] T.M. Miller, J.V. Seeley, W.B. Knighton, R.F. Meads, A.A. Viggiano, R.A. Morris, J.M. Van Doren, J. Gu, H.F. Schaefer III, J. Chem. Phys. 109 (1998) 578.
[4] D.H. Williamson, C.A. Mayhew, W.B. Knighton, E.P. Grimsrud, J. Chem. Phys. 113 (2000) 11035.
[5] W.B. Knighton, T.M. Miller, E.P. Grimsrud, A.A. Viggiano, J. Chem. Phys. 120 (2004) 211.
[6] B.P. Mathur, E.W. Rothe, S.Y. Tang, G.P. Reck, J. Chem. Phys. 65 (1976) 565.
[7] T.M. Miller, A.A. Viggiano, R.A. Morris, A.E.S. Miller, J. Chem. Phys. 111 (1999) 3309.
[8] A.I. Fernandez, A.J. Midey, T.M. Miller, A.A. Viggiano, J. Phys. Chem. A. 108 (2004) 9120.
[9] A.E. Reed, P.v.R. Schleyer, J. Am. Chem. Soc. 112 (1990) 1434.
[10] J.A. Dobado, H. Martínez-García, J.M. Molina, M.R. Sundberg, J. Am. Chem. Soc. 120 (1998) 8461.
[11] D.B. Chesnut, A. Savin, J. Am. Chem. Soc. 121 (1999) 2335.
[12] C. Yang, E. Goldstein, S. Breffle, S. Jin, J. Mol. Struct. 259 (1992) 345.
[13] A. Nowek, R. Richardson, P. Babinec, J. Leszczyński, J. Mol. Struct. 436 (1997) 419.
[14] C.E. Check, K.C. Lobring, P.R. Keating, T.M. Gilbert, L.S. Sunderlin, J. Phys. Chem. A. 107 (2003) 8961.
[15] L.S. Sunderlin, in: N. Adams, L. Babcock (Eds.), Advances in Gas-Phase Ion Chemistry, vol. 4, JAI Press, Greenwich, CT, 2001, p. 49.
[16] F. Muntean, P.B. Armentrout, J. Chem. Phys. 115 (2001) 1213, and references therein.
[17] P.B. Armentrout, J. Am. Soc. Mass Spectrom. 13 (2002) 419.
[18] K. Do, T.P. Klein, C.A. Pommerening, L.S. Sunderlin, J. Am. Soc. Mass Spectrom. 8 (1997) 688.
[19] K.M. Ervin, P.B. Armentrout, J. Chem. Phys. 83 (1985) 166;
M.T. Rodgers, K.M. Ervin, P.B. Armentrout, J. Chem. Phys. 106 (1997) 4499.
[20] S.K. Loh, D.A. Hales, L. Lian, P.B. Armentrout, J. Chem. Phys. 90 (1989) 5466;
R.H. Schulz, K.C. Crellin, P.B. Armentrout, J. Chem. Phys. 113 (1991) 8590.
[21] C.E. Check, T.O. Faust, J.E. Bailey, B.J. Wright, T.M. Gilbert, L.S. Sunderlin, J. Phys. Chem. A 105 (2001) 8111.
[22] E.G. Robertson, D. McNaughton, J. Phys. Chem. A 107 (2003) 642.
[23] P.B. Armentrout, J. Simons, J. Am. Chem. Soc. 114 (1992) 8627.
[24] Gaussian 98, Revision A.9: M.J. Frisch, G.W. Trucks, H.B. Schlegel, G.E. Scuseria, M.A. Robb, J.R. Cheeseman, V.G. Zakrzewski, J.A. Montgomery, Jr., R.E. Stratmann, J.C. Burant, S. Dapprich, J.M. Millam, A.D. Daniels, K.N. Kudin, M.C. Strain, O. Farkas, J. Tomasi, V. Barone, M. Cossi, R. Cammi, B. Mennucci, C. Pomelli, C. Adamo, S. Clifford, J. Ochterski, G.A. Petersson, P.Y. Ayala, Q. Cui, K. Morokuma, A.D. Malick, K.D. Rabuck, K. Raghavachari, J.B. Foresman, J. Cioslowski, J.V. Ortiz, A.G. Baboul, B.B. Stefanov, G. Liu, A. Liashenko, P. Piskorz, I. Komaromi, R. Gomperts, R.L. Martin, D.J. Fox, T. Keith, M.A. Al-Laham, C.Y. Peng, A. Nanayakkara, M. Challacombe, P.M.W. Gill, B. Johnson, W. Chen, M.W. Wong, J.L. Andres, C. Gonzalez, M. Head-Gordon, E.S. Replogle, J.A. Pople. Gaussian, Inc., Pittsburgh, PA, 1998.
[25] NBO 5.0.: E.D. Glendening, J.K. Badenhoop, A.E. Reed, J.E. Carpenter, J.A. Bohmann, C.M. Morales, F. Weinhold, Theoretical Chemistry Institute, University of Wisconsin, Madison WI, 2001. http://www.chem.wisc.edu/∼nbo5.
[26] M.T. Rodgers, P.B. Armentrout, J. Chem. Phys. 109 (1998) 1787.
[27] J. Sánchez Márquez, M. Fernández Núñez, J. Mol. Struct. 624 (2003) 239.
[28] E.A. Robinson, R.J. Gillespie, Inorg. Chem. 42 (2003) 3865, and references therein.
[29] A. Begum, M.C.R. Symons, J. Chem. Soc. A (1971) 2065.
[30] P.H. Svensson, L. Kloo, Chem. Rev. 103 (2003) 1649.
[31] C. Hao, J.D. Kaspar, C.E. Check, K.C. Lobring, T.M. Gilbert, L.S. Sunderlin, J. Phys. Chem., submitted for publication.
[32] G.P. Dudchik, O.G. Polyachenok, Russ. J. Inorg. Chem. 24 (1979) 360.
[33] M. Binnewies, M. Lakenbrink, H. Schnöckel, Z. Anorg. Allg. Chem. 497 (1983) 7.
[34] M.W. Chase, Jr., NIST-JANAF Themochemical Tables, fourth edition, J. Phys. Chem. Ref. Data, Monograph 9, 1998.
[35] M. Binnewies, Z. Anorg. Allg. Chem. 507 (1983) 66.
[36] M.F. Mole, J.C. McCoubrey, Nature 202 (1964) 450.
[37] H. Schnöckel, M. Lakenbrink, Z. Anorg. Allg. Chem. 507 (1983) 70.
[38] S. Firth, R.W. Davis, J. Mol. Spectrom. 127 (1988) 209.
[39] S. Firth, R.W. Davis, J. Mol. Spectrom. 179 (1996) 32.
[40] B. Brupbacher-Gatehouse, T. Brupbacher, J. Chem. Phys. 111 (1999) 6300.
[41] I.S. Bell, P.A. Hamilton, P.B. Davies, J. Mol. Spectrosc. 200 (2000) 287.